Conformational Dynamics of Single G Protein-Coupled Receptors in Solution

Samuel Bockenhauer,[†,‡,∥] Alexandre Fürstenberg,[†,∥] Xiao Jie Yao,[§,∥] Brian K. Kobilka,[§,∥] and W. E. Moerner[*,†,∥]

[†]Department of Chemistry, Stanford University, Stanford, California 94305, United States

[‡]Department of Physics, Stanford University, Stanford, California 94305, United States

[§]Department of Molecular and Cellular Physiology, Stanford University School of Medicine, Stanford, California 94305, United States

Ⓢ Supporting Information

ABSTRACT: G protein-coupled receptors (GPCRs) comprise a large family of seven-helix transmembrane proteins which regulate cellular signaling by sensing light, ligands, and binding proteins. The GPCR activation process, however, is not a simple on−off switch; current models suggest a complex conformational landscape in which the active, signaling state includes multiple conformations with similar downstream activity. The present study probes the conformational dynamics of single β_2-adrenergic receptors (β_2ARs) in the solution phase by Anti-Brownian ELectrokinetic (ABEL) trapping. The ABEL trap uses fast electrokinetic feedback in a microfluidic configuration to allow direct observation of a single fluorescently labeled β_2AR for hundreds of milliseconds to seconds. By choosing a reporter dye and labeling site sensitive to ligand binding, we observe a diversity of discrete fluorescence intensity and lifetime levels in single β_2ARs, indicating a varying radiative lifetime and a range of discrete conformational states with dwell times of hundreds of milliseconds. We find that the binding of agonist increases the dwell times of these states, and furthermore, we observe millisecond fluctuations *within* states. The intensity autocorrelations of these faster fluctuations are well-described by stretched exponential functions with a stretching exponent $\beta \sim 0.5$, suggesting protein dynamics over a range of time scales.
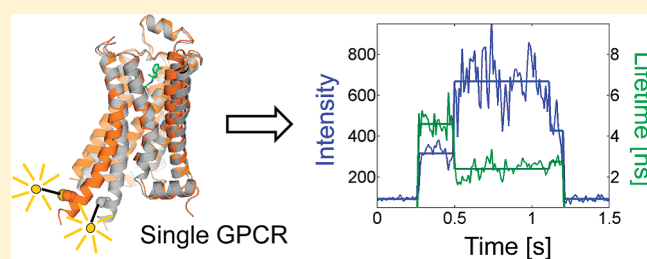
■ INTRODUCTION

G protein-coupled receptors (GPCRs) form a class of over 800 membrane proteins that regulate a large variety of physiological processes by specifically transducing signals (photons, ions, small molecules, and peptide and protein hormones) from the outside to the inside of a cell.[1,2] At the molecular level, all GPCRs share a conserved tertiary structure with seven transmembrane α-helical motifs (TMs), the *N*-terminus outside the cell, and the *C*-terminus on the cytosolic side of the cell membrane. Agonists bind to the interior of the hydrophobic TMs on the extracellular surface, initiating subtle conformational changes which propagate to the intracellular surface. This transmitted "signal" stimulates binding and activation of G proteins on the intracellular receptor side. G protein activation in turn triggers downstream signaling cascades, controlling a broad range of important physiological processes. For this reason, GPCRs have been preferential therapeutic targets for a wide spectrum of diseases.[3,4]

Despite their widespread use as drug targets, the detailed molecular mechanisms by which ligand binding modulates GPCR activity remain poorly understood. Like most proteins,[5,6] GPCRs are highly dynamic entities that exist in multiple atomic-scale conformations. They do not act as simple "on−off" switches, but rather like fluctuating integrators of information.[4,7] Even in the ligand-free basal state, they constantly switch between an inactive state (R) and an active state (R*) which can engage the G protein,

with each state comprising an ensemble of various conformations.[5,8] Ligand binding modulates the receptor function by displacing the conformational equilibrium. Agonists (activating ligands) stabilize conformations which increase G protein-mediated signaling; inverse agonists (inhibiting ligands) stabilize different conformations which decrease the basal level of signaling.[2] Structurally very similar ligands can drive the conformational ensemble to diverse equilibria and trigger very different physiological responses.[8−11]

Recent structural studies of ligand-activated GPCRs have provided some insight into the mechanisms of activation.[2,12−20] An important breakthrough was achieved early this year with the report of the first series of high-resolution crystal structures of ligand-activated GPCRs obtained in the presence of various receptor agonists.[21−23] Surprisingly, these studies found that the G protein is required to stabilize the active state: in its absence, the agonist-bound GPCRs crystallized in the inactive R state. Solution studies have however shown the ability of agonists to displace the conformational equilibrium toward the R* state,[9,21,24−26] suggesting that the active conformations are only of transient nature in the absence of G proteins. Inherently dynamic techniques enabling the

capture of transient species are therefore needed to gain insight into the active state conformations.

Single-molecule fluorescence spectroscopy has proven to be a particularly valuable tool to study protein dynamics at the molecular level.[6,27−31] By removing the ensemble averaging inherent in bulk experiments, it directly probes the underlying heterogeneity which often arises for biomolecules, for example, if the various individual copies of a protein are in different conformations. It further allows unsynchronized or rare events such as transition states to be monitored in addition to average behavior.[32−36]

Prolonged observation of single molecules in solution at room temperature in a close-to-native environment has nonetheless been challenging because Brownian motion causes nanoscale objects to diffuse quickly out of the confocal detection volume. Surface immobilization by chemical means has often been used to eliminate this problem, but there remains persistent doubt as to whether surface-attached molecules behave the same as free-solution molecules,[37] particularly when the goal is to probe subtle conformational changes and photodynamics. While laser tweezers can trap objects in solution in the $100-1000$ nm range,[38] the optical trapping force (scaling with volume) is insufficient to trap smaller objects of size <10 nm, including most proteins. On the other hand, the Anti-Brownian ELectro-kinetic (ABEL) trap has demonstrated its ability to study single biomolecules free in solution at ambient conditions for prolonged periods of time.[39−43] The ABEL trap combines fluorescence-based position estimation with fast electrokinetic feedback to oppose the Brownian motion of a single nanoscale object, hence maintaining its position in the field of view *without* perturbing its internal degrees of freedom. Current implementations have allowed stable trapping of single-dye-labeled DNA oligomers[44] and single organic dyes[45] for several seconds, with the trapping time limited only by the photobleaching of the dye. Moreover, as opposed to the case with fluorescence correlation spectroscopy (FCS),[46] the molecule is trapped in a region of time-averaged uniform intensity so that useful information can be extracted from the brightness. For example, light-induced conformational changes and fluctuations in the intrinsic chromophore radiative rate for trapped allophycocyanin protein molecules have recently been observed using an ABEL trap; these findings would not have been observable in bulk experiments and differ substantially from previous single-molecule studies in which the same protein had been immobilized in polymers or on a glass surface.[42]

We describe in this work our use of an ABEL trap to investigate the conformational dynamics of detergent-solubilized single molecules of the β_2-adrenergic receptor (β_2AR), a canonical GPCR involved in smooth muscle regulation, in the presence and in the absence of the full agonist BI-167107. Detergent-solubilized β_2AR labeled with tetramethylrhodamine (TMR) at the end of TM6 (Figure 1) was previously shown to respond in a ligand-specific way to the binding of agonists by undergoing conformational changes which selectively modulate the fluorescence quantum yield of the probe,[9] a metric known to depend on the local environment of the fluorophore.[47,48] This picture of multiple distinct substates induced by different ligands has further been confirmed by experiments using plasmon-waveguide resonance.[49] An earlier attempt to probe freely diffusing β_2AR obtained indirect evidence for a distribution of more than one conformational state but was unable to resolve dynamics for each molecule due to the ~ms transit time of each receptor through the confocal probe volume.[50] In the present
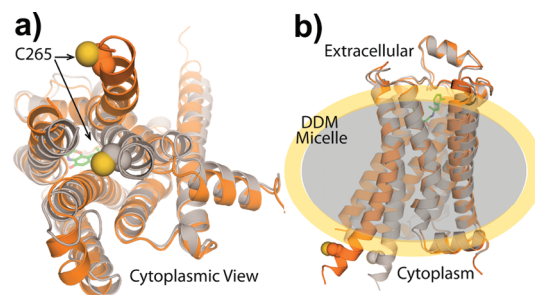

Figure 1. Structure of β_2AR-TMR in active (orange) and inactive states (gray). Panel (a) shows a cytoplasmic view with the TMR labeling location indicated by space-filling spheres. Panel (b) shows the side view with the full agonist BI-167107 (small green structure on extracellular side) and a sketch of the surrounding *n*-dodecylmaltoside (DDM) detergent micelle (shaded).

study, however, we perform ABEL trapping of single β_2AR molecules in the absence of G proteins for hundreds of milliseconds to seconds, during which time we simultaneously measure both the fluorescence intensity and the excited-state lifetime for every trapped receptor, which change discontinuously with time at the single-receptor level. By combining the observed correlated lifetime-intensity measurements for all molecules, we find a complex conformational landscape as evidenced by a diversity of discrete values for fluorescence intensity and lifetime. These states interconvert on time scales of hundreds of milliseconds, indicating changes in the local protein environment as probed by the fluctuating radiative and nonradiative lifetimes of the TMR reporter dye. We find that agonist binding causes a clear shift in the equilibrium distribution of these states. In addition, agonist binding increases the dwell times within states and reduces the local flexibility of the receptor. We thus obtain the first experimental dynamic insights into conformational fluctuations for single β_2AR in solution.

■ METHODS

Sample Preparation. β_2AR in which four reactive cysteines were mutated (C77V, C327S, C378A, and C406A) was expressed in Sf9 insect cells, solubilized, and purified by affinity chromatography according to previously described procedures.[51] The purified receptor was incubated with an equivalent amount of tetramethylrhodamine-5-maleimide (TMR, single isomer, T-6027, Invitrogen) for 30 min at room temperature. The TMR-labeled receptor (β_2AR-TMR) was then purified by gel filtration immediately before use, usually resulting in $1-3$ μM solutions. Agonist-bound β_2AR-TMR was prepared by incubation of $1-3$ μM receptor solution with a 10-fold stoichiometric excess of the full agonist BI-167107[21] for 2 h at 4 °C immediately prior to experiments. BI-167107 was chosen for its ~nM dissociation constant and extremely slow ~$(150 \text{ h})^{-1}$ off-rate, enabling extended study in the ABEL trap at single-molecule concentrations. The ligand-free and the agonist-bound receptor stock solutions were used directly for bulk spectroscopy, whereas for trapping experiments, they were diluted by $4-5$ orders of magnitude. All samples were handled in PBS buffer (Gibco 10010) at pH 7.4 supplemented with 0.1% (w/w) *n*-dodecyl-maltoside (DDM, Anatrace) and stored on ice in the dark. Experiments were conducted as soon as possible after labeling. Ligand-free and agonist-bound data sets included two independent receptor preparations with multiple ensemble and trapping experiments for each preparation.

Ensemble Measurements. All measurements were performed in a 1 cm quartz low-volume cuvette. Absorption spectra were recorded on a Cary 6000i spectrophotometer (Varian), whereas fluorescence excitation and emission spectra were measured on a Fluoromax-4 fluorescence spectrometer (Horiba). Fluorescence quantum yield measurements were performed using rhodamine 6G in ethanol as a standard ($\Phi_{fl} = 0.94$[52]), and changes in index of refraction were taken into account when necessary.

Excited-state lifetimes were acquired with the time-correlated single-photon counting (TCSPC) technique. Excitation at 515 nm was achieved using the frequency-doubled output of a 1030 nm mode-locked femtosecond fiber laser (Mercury 2000-200-MOD, Polaronyx). The average power was ~0.5 mW at 43 MHz repetition rate with <1 ps pulses. Fluorescence was collected at 90° and passed through a 550 nm long-pass filter (HQ550LP, Chroma) and an analyzer set at the magic angle with respect to the vertical excitation polarization. A Si single-photon detection module with fast timing resolution (PDM-5CTC, Micro Photon Devices) ensured efficient detection. Acquisition was performed with a TCSPC module (PicoHarp-300, Picoquant) connected to a computer with an overall instrument response function (IRF) of ca. 400 ps (full width at half-maximum, fwhm). For time-resolved fluorescence polarization anisotropy experiments, two fluorescence decay traces were recorded with the analyzer set at parallel (VV) and perpendicular (VH) orientation with respect to the excitation polarization. The anisotropy decay $r(t)$ was computed using the standard formula[53]

$$ r(t) = \frac{VV(t) - gVH(t)}{VV(t) + 2gVH(t)} $$

The polarization correction factor g, quantifying the difference in detection efficiency between parallel and perpendicular polarizations, was measured to be 1.0 for our setup. Decays included at least 10^6 total photons with a negligible laser-induced background.

ABEL Trap Experiments. ABEL trap microfluidic cells were assembled by bonding a molded polydimethylsiloxane (PDMS) chamber to a glass coverslip as previously detailed.[54] Before injection into the ABEL trap, diluted samples were combined with the antiadsorption polymer POP6 without denaturant (Applied Biosystems) at 10% (v/v) to prevent the receptors from sticking to the coverslip surface. The presence of the polymer did not affect the photophysics of β_2AR-TMR.

ABEL trapping experiments were performed on an Olympus IX71 inverted microscope equipped with a high-NA oil objective (1.35 NA, 60×, Olympus). The 515 nm pulsed excitation beam (the same as described in ensemble TCSPC measurements, but with an average power of 40 μW before objective) was sent through an orthogonal pair of acousto-optic modulators (46080-3-LTD, NEOS) to deflect the beam along a circular path with an angular frequency of 26 kHz. The circularly revolving beam was then steered into the microscope and imaged to the focal plane with a beam radius of 0.7 μm and revolution radius of 0.3 μm, yielding a time-averaged uniform intensity profile. Fluorescence was detected with a fiber-coupled avalanche photodiode (SPCM-AQ4C, Perkin-Elmer) after filtering through a 545 nm long-pass filter and a 610 nm short-pass filter (HQ545LP, E610SP; Chroma). In such a configuration, illuminated receptors emit fluorescence photons whose detection times depend on the position of the revolving beam; a lock-in scheme implemented on a field-programmable gate array (FPGA, 7833R, National

Instruments) estimated the angular position of the receptor.[55] Based on the angular estimate, feedback voltages of up to ±30 V were applied to the solution with a home-built amplifier using a set of four platinum electrodes to oppose the Brownian motion of the receptor, trapping it until the TMR dye photobleached. The static and uniform electric fields induced by these relatively small voltages across a distance of ~10 μm have been shown to have no effect on single-molecule photophysics.[42]

Data Analysis. All data analysis was performed in MATLAB (The Mathworks, Inc.). For ABEL trap data, the time-tagged photon stream was binned into 10 ms bins to create a time trace of the intensity. We selected trapped receptors by applying an automatic threshold. For a receptor to be included in the analysis, we required (1) that the intensity of each 10 ms bin comprising it was at least 2 standard deviations above the mean background level, (2) that the burst duration was at least 30 ms, and (3) that the burst contain at least 200 photons above background. To accurately set the background level, we hand-selected ~5 s of background photons from the time trace in each 300 s interval of acquired data. These photons determined both the mean background level for the burst selection procedure and the time-resolved background decay for lifetime determination detailed below.

As many bursts in our data set show obvious digital steps from one intensity state to another, we applied the change-point determination algorithm developed by Watkins and Yang[56] to identify different states. The change-point algorithm was configured to include only states lasting at least 30 ms, and the resulting set of states was further filtered to calculate dwell times and fluctuation time scales. To determine the fluorescence lifetime of TMR in each state and in each 10 ms bin, the fitting procedure of Zander et al. was applied.[57] Briefly, a trial single exponential decay with decay constant τ was convolved with the measured IRF (0.4 ns fwhm) of the detection system and then added to the measured background decay (see the Supporting Information, SI). This trial decay function was then optimized according to the maximum likelihood estimation (MLE) algorithm to reproduce the data[57] with the estimated lifetime being the optimal decay constant τ. The color-shift delay between the measured IRF and the experimental decay was included as a free parameter in the fit. The lifetime decay of each 10 ms bin contains a smaller number of photons (typically hundreds rather than thousands), and so the traces are noisier, leading to higher uncertainties in the fitting parameters, but the gain in time resolution allowed us to detect substantial shifts in lifetime even at a relatively constant intensity (Figure 3d). Lifetimes from ensemble measurements were extracted according to the same MLE-based method. The far higher signal-to-background ratio made full background decay correction unnecessary, but a time-independent offset term was included to adjust for dark counts.

Autocorrelations were calculated by combining the time-tagged photons in each state into 50 μs bins. This shorter bin time was chosen for higher time resolution, although time resolution is limited by the revolution period of the excitation beam, $(26 \text{ kHz})^{-1} = 38$ μs, and the detected photon count rate. Estimates of the autocorrelation in the experimentally relevant 100 μs to 1 s time window are insensitive to bin time. The beam revolution produces, as expected, a sharp oscillating component in the autocorrelation (see the SI), but only autocorrelation lags greater than 200 μs, after the oscillation has died out, were included in the fitting and analysis. For additional controls, see the SI. Autocorrelation fluctuation time scales and stretching exponents as well as mean dwell times were extracted by standard

13330

dx.doi.org/10.1021/jp204843r |*J. Phys. Chem. B* 2011, 115, 13328–13338

nonlinear least-squares fitting with all parameters bounded by 0 and infinity.

■ RESULTS

Labeling and Bulk Spectroscopy. We labeled purified receptors with the environment-sensitive dye TMR at the base of the sixth transmembrane helix (Figure 1), a position known from previous studies to be well-suited to sense conformational changes during receptor activation without interfering with receptor function.[9,21,26,50] The two projections in Figure 1 show the cytoplasmic view (a) and the side view (b) of the receptor with the TMR labeling location indicated by space-filling spheres. The active form of the receptor is shown in orange and the inactive form in gray with a shaded ellipsoid around the equatorial region suggestive of the surrounding micelle. We performed bulk absorption, fluorescence, fluorescence quantum yield, fluorescence lifetime, and time-resolved fluorescence polarization anisotropy decay measurements on both ligand-free β_2AR-TMR and β_2AR-TMR incubated with the full agonist BI-167107 to quantify the bulk-level values of these parameters.

No significant change in the absorption spectrum and only a minor blue-shift (4 nm) in the fluorescence spectrum were observed upon agonist binding (Figure S1 of the SI), and the fluorescence quantum yield of the single TMR label increased from 0.33 to 0.38 (Table 1). In correlation with the rise in fluorescence quantum yield, the fluorescence lifetime also increased in the presence of an agonist (Figure 2a). Significantly, the probe on both ligand-free and agonist-bound receptors displays biexponential fluorescence lifetime decays (Table 1), as often observed for fluorescent dyes interacting with proteins,[58,59] indicating heterogeneity in sample or conformation. Ligand-free receptors have 3.6 ns (90%) and 1.6 ns components, whereas agonist-bound receptors have 4.5 ns (95%) and 1.6 ns decay components. The lifetime of TMR is known to increase with decreasing medium polarity,[47,48] likely indicating that TMR explores a less polar microenvironment in the agonist-bound receptor, as already suggested by the hypsochromic shift of the fluorescence. The 1.6 ns component common to both samples could indicate a shared conformation in equilibrium with a more dynamic state whose sensed lifetime increases from 3.6 to 4.5 ns upon activation. However, biexponential fluorescence decays do not necessarily imply the existence of two distinct emitting populations of receptor; they could also originate from a distribution of populations with distinct fluorescence decay times.[60,61] Such closely spaced lifetime states or distributions of lifetimes cannot be resolved from ensemble-averaged measurements.

Bulk measurements of the decay of the fluorescence polarization anisotropy further indicate that the TMR probe senses β_2AR conformational changes, as the decay rate substantially decreases for agonist-bound receptors compared to ligand-free receptors (Figure 2b). Again, the traces are best reproduced by two exponential terms for both samples. Ligand-free receptors exhibit rotational relaxation times of 8.2 ns (74%) and 0.7 ns, whereas the anisotropy of agonist-bound receptors decays with 30 ns (93%) and 0.7 ns time constants. Biexponential fluorescence polarization anisotropy decays are often observed when dyes are attached to macromolecules and generally analyzed using the "wobbling-in-a-cone" model (Table S1 of the SI).[62,63] A fast time scale (0.7−0.8 ns) is used to describe the local wobbling motion of the probe, while a slower time scale (8.2−30 ns) describes tumbling of the macromolecule or of segments of it. In the case of

Table 1. Fluorescence Quantum Yield Φ_{fl}, Excited-State Lifetime Decay Components τ_1 and τ_2 (and Amplitudes), Average Lifetime τ_{av}, and Radiative Lifetime τ_{rad} for β_2AR-TMR in the Absence and in the Presence of BI-167107, All from Bulk Measurements

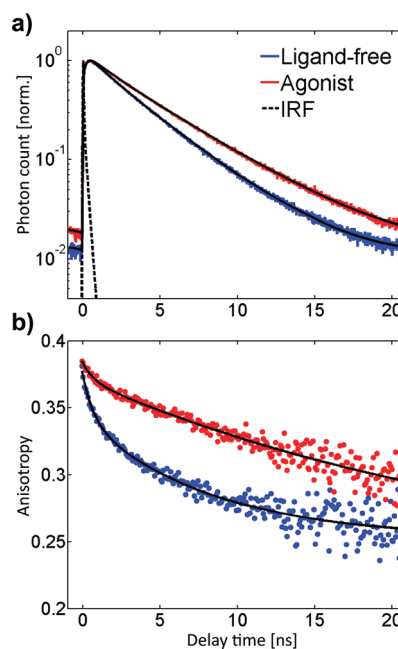| ligand	Φ_{fl}	τ_1 (ns)	τ_2 (ns)	τ_{av} (ns)	τ_{rad} (ns)
ligand-free	0.33 ± 0.02	1.6 (10%)	3.6 (90%)	3.4	10.3
BI-167107	0.38 ± 0.02	1.6 (5%)	4.5 (95%)	4.4	11.6

Figure 2. Bulk fluorescence lifetime (a, 8 ps bins) and time-resolved fluorescence polarization anisotropy decays (b, 80 ps bins) of TMR on ligand-free and agonist-bound receptors. The agonist-bound receptors display a longer fluorescence lifetime and higher anisotropy of the TMR reporter dye.

β_2AR-TMR (Table S1 of the SI), the fraction of fluorescence polarization anisotropy decay associated with TMR wobbling (26%) drastically decreases in the presence of agonist (7%), suggesting that the probe is on average highly confined in agonist-bound conformations. On the other hand, the 30 ns time scale (this value has large uncertainty given that the experimental time window is limited by the excited-state lifetime of the probe) associated with β_2AR tumbling is consistent with the size of a receptor micelle (expected value ∼50 ns). This time scale is not directly observed with ligand-free β_2AR-TMR, which indicates that the 8.2 ns component measured in this case is likely the convolution of two motions, one arising from the motion of a local receptor segment such as the third intracellular loop or TM6, and one from the overall receptor tumbling. This motion attributed to local segment motion becomes totally suppressed in the presence of BI-167107. Our results thus suggest that agonist binding locally stabilizes the receptor into less dynamic and more restricted conformations. These bulk experiments motivate detailed single-molecule investigation of the receptor conformational states and dynamics.

Diversity of Intensity and Lifetime States of Single Receptors. We use the ABEL trap to observe single β_2AR-TMR
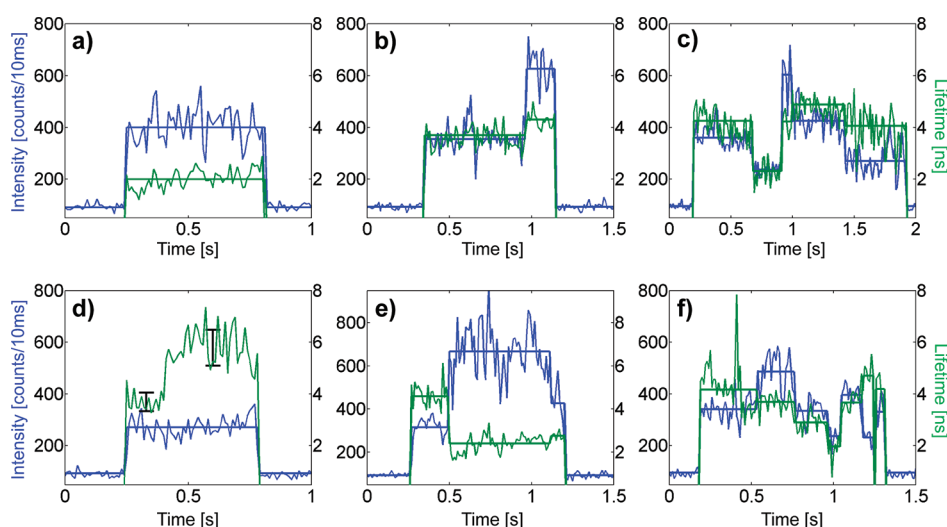
Figure 3. Examples of intensity-lifetime traces with a 10 ms bin size from single trapped ligand-free receptors. Real-time intensity (blue) and fluorescence lifetime (green) are shown with calculated intensity change-point states overlaid (thick lines). Transitions among a range of intensity-lifetime states are observed, in which intensity may be correlated (b,c), uncorrelated (d), or anticorrelated (e) with lifetime. Because trace d shows a large, uncorrelated change in lifetime for constant intensity, we replace the thick line for mean lifetime with 1σ error bars calculated from the 10 ms binned lifetime.

molecules in solution for prolonged periods of time.[39] The design of the ABEL trap is such that a trapped TMR-labeled receptor experiences a spatially uniform excitation profile on a time scale slower than $\sim$200 μs, and for this reason, any observed fluorescence intensity fluctuations can be attributed to intrinsic fluctuations of the TMR-receptor system. In addition, pulsed excitation combined with time-tagging of each detected photon allowed us to calculate both the mean excited-state lifetime of TMR for each trapped receptor, as well as a running estimate of the lifetime for every 10 ms bin. Measuring excited-state lifetime concurrently with fluorescence intensity for each single molecule provides not only correlated values but also an added experimental dimension, enabling, for example, direct access to the intrinsic radiative lifetime. Such correlated measurements cannot be obtained from ensemble studies.

Figure 3 shows six trapped ligand-free receptors exhibiting a representative range of behaviors. Fluorescence intensity (blue) and fluorescence lifetime (green) are plotted on the same time axis with 10 ms bins, where the initial increase represents the initial entry of a single molecule into the trap. The most striking feature of the data is the presence of discrete intensity steps. Given these evident digital transitions, we applied the change-point finding algorithm of Watkins and Yang[56] to statistically identify the time points ("change-points") during which the intensity of a trapped receptor changes significantly. Hereafter we use the word "state" to describe the microscopic conformation of the single receptor in between such change-points, as reported by the mean fluorescence intensity, mean lifetime, and mean fluctuation time scales (see below) of the fluorescence photons from the TMR reporter dye. Our implementation of the change-point algorithm provides an automatic way to identify and catalog receptor states consistent with those that might be chosen by eye. The 10 ms binned data indicates the calculated intensity (blue) and lifetime (green) in every 10 ms interval, whereas the heavy, straight lines indicate change-point mean intensity states and the much more accurate mean lifetime value calculated from pooling together and fitting the decay from all photons in the state.

The largest fraction ($\sim$90%) of trapped receptors remain in a single intensity state until the TMR dye photobleaches (Figure 3a). The remaining $\sim$10% of receptors show state-to-state dynamics with a range of different behaviors. Figure 3b shows a clear step upward in intensity, combined with a small correlated increase in lifetime. In Figure 3c, the trapped receptor exhibits multiple intensity steps with closely correlated changes in lifetime. Other receptors, however, displayed large changes in probe lifetime even at constant intensity (Figure 3d). Instances of clear anticorrelation between intensity and probe lifetime were also observed (Figure 3e). Unusually, these behaviors indicate a sudden, substantial change in the radiative lifetime of the probe. In some cases, single receptors undergoing lifetime transitions both correlated and anticorrelated with intensity could be monitored (Figure 3f). Taken together, the different single-molecule examples in Figure 3 show that the various different receptors sample a range of discrete intensity-lifetime states. It would be ideal to be able to observe one single receptor for far longer times to see if each receptor can sample all possible states. Since this is not possible due to the eventual photobleaching of the probe, we make the reasonable assumption that each receptor is only sampling a portion of the states available.

We observed qualitatively similar behavior for both ligand-free (3962 receptors trapped and observed) and agonist-bound receptors (4312 receptors trapped and observed); by eye, individual trapped receptors from both groups cannot be distinguished. Quantitative analysis of the correlated fluorescence intensity-lifetime values observed for all molecules, however, revealed substantial differences. Figure 4 represents a two-dimensional density plot (histogram) of the observed distribution of intensity-lifetime states for both ligand-free and agonist-bound receptors, with representative fitted excited-state lifetime decays from two specific locations in the plot. In agreement with bulk measurements, the agonist-bound receptors display higher mean intensity and higher mean lifetime compared to the ligand-free receptors. The peak of the distribution is likewise at higher intensity and lifetime for the agonist-bound receptors. The
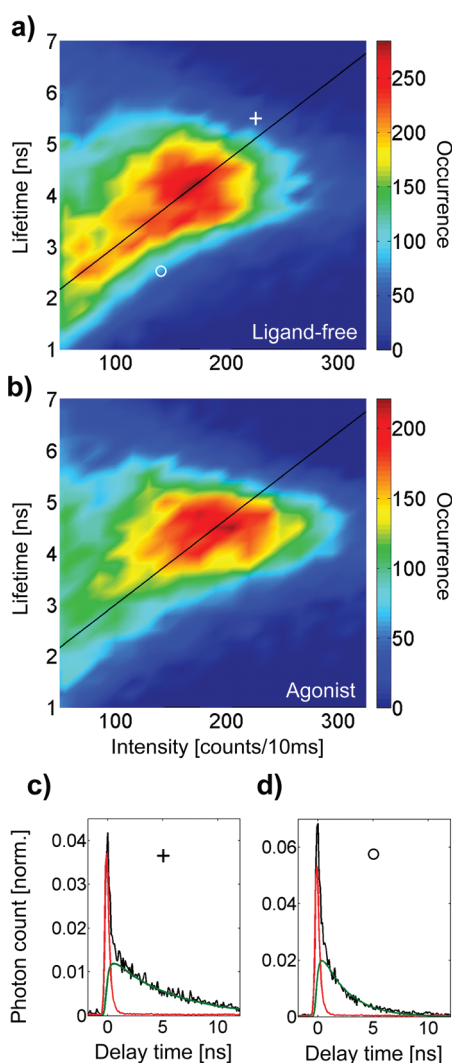
Figure 4. Peak-normalized density plots of the intensity-lifetime states for the full population of ligand-free (a) and agonist-bound single receptors (b). The color bar indicates the number of states observed in each $(15 \text{ cts}/10 \text{ ms}) \times (0.25 \text{ ns})$ bin. Agonist-bound receptors show a tighter distribution of states with higher peak intensity and lifetime compared to ligand-free receptors. The diagonal line is a guide to the eye, highlighting states of constant radiative lifetime. In c and d, we show typical lifetime decays (black) from states at coordinates ○ and +, which include the fitted lifetime component (green) together with the background component (red).

ligand-free receptors show a broad distribution of states from low intensity and low lifetime to high intensity and high lifetime, including a peak near 170 counts per bin and 4 ns. The agonist-bound receptors, however, explore far fewer states at low intensity and low lifetime, although the rough linear trend of positive correlation remains visible. The peak region of the agonist-bound distribution is narrower in lifetime, but with greater spread along the intensity axis, evident in the oblong peak shape. To probe changes in radiative rate, we note that the intensity I and the excited-state lifetime τ can be written as usual as

$$I \propto \Phi_{fl} = \frac{k_{rad}}{k_{rad} + k_{nrad}}; \quad \tau = \frac{1}{k_{rad} + k_{nrad}}$$
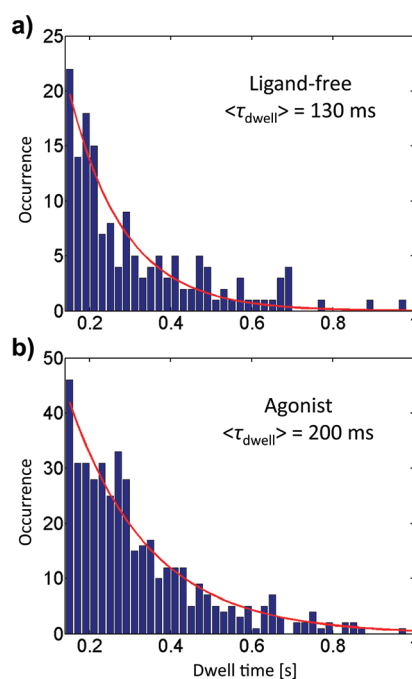

Figure 5. Histograms of state dwell times for the full population of ligand-free (a) and agonist-bound receptors (b). The mean dwell times are estimated from a single exponential fit with time constant τ_{dwell}. Agonist-bound receptors show longer state dwell times than ligand-free receptors.

where k_{rad} is the intrinsic radiative rate and k_{nrad} is the nonradiative (quenching) rate. Dividing these equations yields the radiative rate alone, up to a constant which depends on the detection efficiency of the setup. We also assume that the absorption spectrum, and therefore the excitation rate, remains constant for the TMR-receptor system, as bulk absorption spectra of ligand-free and agonist-bound receptors are extremely similar (Figure S1, Supporting Information). Thus, as a guide to the eye, we plot a diagonal line to highlight states of constant radiative lifetime, $\tau_{rad} = k_{rad}^{-1} \propto \tau/I$. States at different coordinates along the line experience varying degrees of nonradiative quenching with correlated lifetime and intensity, whereas states far from the line exhibit a different radiative lifetime. Distributions for both samples have detailed structure and high asymmetry and do not show obvious clustering into well-resolved peaks, making them inconsistent with a single ligand-free (inactive) or a single agonist-bound (active) state. Indeed, the range of intensity-lifetime states along the line of constant radiative lifetime provides evidence for a range of discrete conformational substates in which the TMR probe experiences slightly different microenvironments.

Time Scales of Conformational Dynamics. In addition to probing the equilibrium distribution of fluorescence intensity-lifetime states, the prolonged observation time provided by ABEL trapping allowed us likewise to investigate the dynamics. In Figure 5, we examine the distribution of state dwell times, defined as the residence time of the receptor in a given state before it transitions to a different state. An essential caveat is that transitions among receptor states occur independently of trapping; residence in a state does not begin when the receptor is trapped, nor does it end when the TMR probe photobleaches. Thus, to obtain an unbiased dwell time distribution, we included only dwell times of the intermediate time states (not first or last)
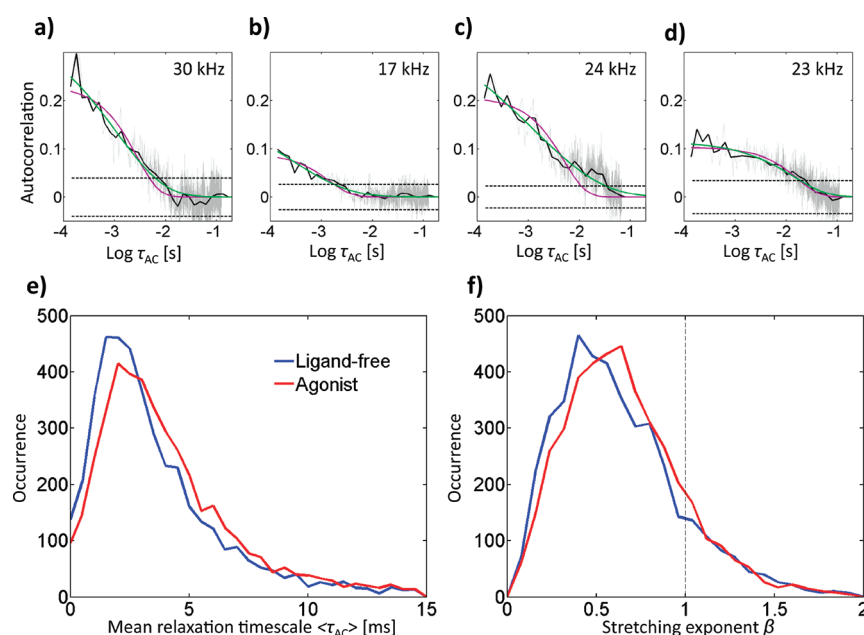
Figure 6. Intensity autocorrelation of individual intensity-lifetime states longer than 200 ms. We show example autocorrelations (a, b, c, d) calculated with linear bins (gray) and logarithmic bins (black), and we include 95% confidence bounds on zero (dashed) and the mean signal photon count rate of the state (upper right). The autocorrelation (a) is from the state in Figure 3a, and the autocorrelation (b) is from the state in Figure 3d. We use a stretched exponential fit (green) rather than a single exponential fit (purple) because it more accurately describes the data. We show histograms of mean decay times (e) and stretching exponents (f) for ligand-free and agonist-bound receptors.

of trapped receptors traversing at least three states. Furthermore, because the accuracy of the change-point algorithm increases for longer-lived states due to more data, we have highest confidence in long dwell times.[56] On the other hand, shorter states are more numerous, allowing more robust statistics and fitting. As a compromise, we took into account only states lasting at least 150 ms. The agonist-bound receptors show a clear increase in mean dwell time (200 ms, extracted from a single-exponential fit) compared with the ligand-free receptors (130 ms). Equivalently, transitions between states occur less often, on average, in agonist-bound receptors.

Although our use of the change-point algorithm accurately identifies large changes in intensity, it does not simultaneously capture smaller, faster fluctuations. The state in Figure 3a and the second state in Figure 3e, for example, display large fluctuations *within* single identified states. Indeed, more than 90% of states in both samples show fluctuations in excess of shot noise (data not shown). To characterize these faster fluctuations, we computed the intensity autocorrelation of the photons comprising each state.

The intensity autocorrelation $G(\tau_{AC})$ of a time-varying intensity trace essentially describes, on average, how much the intensity changes between time t and time $t + \tau_{AC}$, as a function of the lag time τ_{AC}. High values of $G(\tau_{AC})$ indicate small change (high correlation), whereas low values of $G(\tau_{AC})$ indicate significant change (low correlation). Most dynamic physical systems show a smooth decay between high correlation at short times and low correlation at long times; examination of this decay provides access to the underlying dynamical time scale. For each state, we calculate the intensity autocorrelation

$$G(\tau_{AC}) = \langle \delta I(t + \tau_{AC}) \delta I(t) \rangle$$

where τ_{AC} is the autocorrelation time, $\langle...\rangle$ denotes averaging over the intensity trace, and $\delta I(t) = I(t) - \langle I(t) \rangle$ is the mean-

subtracted intensity. Intensity autocorrelation finds wide application in FCS,[46] where it is used to quantify, among other quantities, the mean transit time of a fluorescent object through a confocal excitation volume of known size, allowing extraction of the diffusion coefficient of the object. More generally, autocorrelation can be used to quantify conformational dynamics,[32,64] or indeed any time-dependent fluctuation, but in typical FCS experiments, the dynamics from many single molecules are averaged, as opposed to the case here. An on–off telegraph signal with mean relaxation time $\bar{\tau}_{AC}$ will have theoretical intensity autocorrelation $G(\tau_{AC}) \propto \exp(-\tau_{AC}/\bar{\tau}_{AC})$, and as such the single exponential form is often used to estimate the mean relaxation time scale $\langle \tau_{AC} \rangle$ of a fluctuation process.[64] Note that in this instance, $\langle...\rangle$ indicates averaging over the autocorrelation decay, not averaging over the intensity trace.

Figure 6 shows four representative autocorrelations obtained from four ligand-free receptor states. To accurately estimate the autocorrelation on millisecond time scales (see below), only states of at least 200 ms duration were included in the autocorrelation analysis. In each case, the average photon detection count rate was sufficient to detect fluctuations on the time scale plotted. We plot the intensity autocorrelation (light gray), calculated up to $\tau_{AC} = t_{max}/4$, where t_{max} is the duration of the state, as recommended by Box and Jenkins.[65] The uncertainty in the calculated autocorrelation increases at higher time lags τ_{AC} as a result of poorer sampling; to counteract this effect, we performed all fits on the logarithmically binned autocorrelation (solid black line) to more robustly sample the longer time lags. We also plot confidence intervals about zero (dashed line, 95% confidence) to confirm the existence of positive autocorrelation above noise.[65−67] According to this test, greater than 97% of states longer than 200 ms displayed significant autocorrelation; the remainder were excluded from further analysis.

Single exponential decays fail to adequately describe most autocorrelations (Figure 6a–d). A better fit to the data is provided by the stretched exponential form

$$G(\tau_{AC}) \propto \exp((-\tau_{AC}/\overline{\tau}_{AC})^\beta)$$

where $0 < \beta < 1$ is the stretching exponent and $\overline{\tau}_{AC}$ is the characteristic time scale.[68] The stretched exponential form can be interpreted as a superposition of multiple exponentials and thus describes a distribution of time scales, increasingly broadened as β decreases from 1. In contrast to the single exponential form, for which the characteristic time $\overline{\tau}_{AC}$, a parameter of the fit, is equal to the mean relaxation time scale $\langle \tau_{AC} \rangle$, the mean relaxation time scale of a stretched exponential is obtained from $\langle \tau_{AC} \rangle = (\overline{\tau}_{AC}/\beta)\, \Gamma(1/\beta)$, where $\Gamma(x)$ denotes the gamma function. It is the single-molecule distribution of this (more physical) quantity for ligand-free and agonist-bound receptors which is represented in Figure 4e. Both distributions are similarly broad and asymmetric, peaking around 2 ms, although agonist-bound receptors show a slight shift to longer time scales. This time scale is too slow to arise from motion of the probe around its linker in the nanosecond regime (Figure 2b), and we thus attribute these observed intensity fluctuations to intrinsic fluctuations of the receptor. The distributions of the stretching exponent β in Figure 4g are again similar for both samples, peaking around $\beta \sim 0.5$, although the agonist-bound receptors show a slight shift toward higher β, indicating a tighter distribution of time scales (closer to single exponential at $\beta = 1$). The broadness of the β distribution is due to the difficulty of estimating stretched exponential parameters from short time series. Indeed, Lu et al. find substantial broadening in β distributions for single-molecule intensity traces, although for time series at least 100 times longer than the characteristic autocorrelation time scale, the peak β provides an accurate estimate for the true β.[69] Given our fluctuation time scale of $\sim$2 ms and state duration of at least 200 ms, we expect an accurate estimate of β from its peak value. We confirmed that no correlation exists between dwell time and mean relaxation time for either sample, thus ruling out the possibility that relaxation time scales may be influenced by artifacts of sampling. Indeed, we find that peak time scales obtained from the stretched exponential fits are the same as those obtained from single exponential fits (data not shown). The fact that the vast majority of extracted β values are decidedly less than 1, however, is strong evidence that the stretched exponential form provides a more accurate description of the data.

■ DISCUSSION

By labeling the end of TM6 with the environment-sensitive fluorescent probe TMR, we were able to experimentally follow the conformational dynamics of β_2AR, a model GPCR, in the absence and in the presence of the full agonist BI-167107. The cytoplasmic end of TM6 is particularly well-suited to sense conformational changes as this segment undergoes a large outward movement of 11 Å upon transition of the receptor from an inactive to an active state,[21] and TMR was shown in this and previous studies to selectively report on agonist-induced conformational transitions by having its fluorescence quantum yield, fluorescence lifetime, or fluorescence polarization anisotropy decay modulated.[9,70,71] Our results suggest that the probe experiences a less polar, conformationally more restricted environment in the agonist-bound form of the receptor. The mechanism by which TMR senses changes in its environment is related

to polarity, the fluorescence quantum yield and lifetime increasing with decreasing polarity.[47,48] The longest reported lifetime for TMR in apolar media is 3.7 ns, a value close to the mean lifetime of ligand-free β_2AR-TMR measured here (3.4 ns). We observe, however, an even longer mean lifetime of 4.4 ns for agonist-bound β_2AR-TMR, incompatible with a solely polarization-related mechanism. Radiative lifetime fluctuation arising from modulation of the refractive index and hyperpolarizability of the environment of the dye due to nanoconfinement could account for this observation and act as a second fluorescence contrast mechanism.[72] The very slow decay of the fluorescence polarization anisotropy of agonist-bound β_2AR-TMR due to quasi-absence of TMR wobbling motion is consistent with nanoconfinement of the probe. This mechanism would also support the changes in radiative lifetime witnessed both in ensemble (Table 1) and in single-molecule (Figure 3) measurements, as neither changes in the orientation of the dipole moment of the probe nor spectral shifts can account for this observation in the solution phase.[73]

Although we do not have a crystal structure showing the actual position of the fluorescent probe relative to the atomic positions of the GPCR, we can speculate on the origins of the fluorescence changes observed in this work. In the inactive form (gray in Figure 1), the labeling position is nestled among the helices of the protein, while in the active form (orange in Figure 1), the labeled helix extends outward and rotates. Although this position may appear more hydrophilic, the increased rigidity and hydrophobicity we observe for agonist-bound GPCR may be due to the ability of the probe on its linker to interact more strongly with the nearby detergent molecules. Rearrangement of the micelle itself is expected to take place on time scales of tens of nanoseconds or faster and cannot account for that effect.[74−76]

The account of receptor dynamics which emerges from single-molecule experiments confirms the complexity of the conformational landscape of GPCRs and, consistent with other observations, rules out any simple two-state activation model.[7] The numerous distinct states that ligand-free β_2AR explores (Figure 4a) reflect the mechanism underlying the constitutive activity of the receptor; even in the absence of an agonist, β_2AR switches between several inactive and active conformations. The striking feature of Figure 4a, analogous to a state map obtained along one conformational coordinate (i.e., that probed by TMR), however, is its lack of clear local structure which could allow conformations to be grouped together and discrete intermediates in the activation pathway of the receptor to be defined. Our data rather suggest the existence of a large number of discrete states along the activation pathway. Agonist binding displaces the equilibrium toward active conformations (Figure 4b), but as suggested by molecular dynamics simulations,[22] this event alone is not sufficient to lock the receptor into active states, even if it seems to lead to a partial stiffening of the protein as suggested by the longer average dwell time (Figure 5) and the fluorescence polarization anisotropy data (Figure 2b). Although agonist binding lowers the difference in energy between inactive and active conformations, inactive conformations remain energetically favored in the absence of the G protein,[22] hence the similarities in the behaviors observed on the single-receptor level in the presence and in the absence of agonist. The dynamic nature of β_2AR is reinforced by the millisecond-time scale fluctuations recorded within fluorescence intensity and lifetime states. The fact that a distribution of time scales is needed to accurately describe these fluctuations is consistent with a

13335

dx.doi.org/10.1021/jp204843r |*J. Phys. Chem. B* 2011, 115, 13328–13338

complex and dynamic conformational landscape encompassing numerous distinct states.[77]

■ CONCLUSION

In this work we present the first single-molecule study of β_2AR conformational dynamics in solution. By permitting observation of single receptors for prolonged times, the ABEL trap allows us to access not only the distributions of conformational states, but also their interconversion rates and fast fluctuations. The novel single-molecule results of this work are the following: direct experimental observation of both discrete, stepwise as well as fluctuating conformational dynamics as reported by intensity and lifetime of TMR in single receptors (Figure 3); the first two-dimensional "map" of the shift in conformational equilibria in the ensemble caused by agonist binding, represented in correlated intensity-lifetime space (Figure 4); and measurement of time scales of interconversion of these states over 3 orders of magnitude, milliseconds to seconds, which have proved inaccessible to other techniques (Figures 5 and 6). These results suggest a rugged, dynamic energy landscape consistent with the highly evolved GPCR cellular regulation mechanisms known from structural and biochemical assays. On the other hand, evidence for multiple interconverting conformational substates is only a statement of the problem; more work is needed to resolve discrete atomic-scale conformations and to integrate them into a more complete dynamical model of G protein activation. Our results additionally suggest that fluctuations in the radiative rate could serve as a novel probe of the protein dielectric microenvironment.

■ ASSOCIATED CONTENT

Ⓢ Supporting Information. Details of absorption and fluorescence spectroscopy for quantum yield determination, single-molecule lifetime fitting, autocorrelation analysis and controls, and bulk anisotropy measurements. This material is available free of charge via the Internet at http://pubs.acs.org.

■ AUTHOR INFORMATION

Present Addresses
[⊥]Department of Structural Biology and Bioinformatics, University of Geneva, 1211 Genève 4, Switzerland.

■ AUTHOR INFORMATION

Author Contributions
[∥]S.B. and A.F. contributed equally to this work. S.B, A.F., B.K.K, and W.E.M. conceived and designed experiments; S.B. performed ABEL trap experiments; A.F. performed bulk experiments; X.J.Y. and B.K.K. expressed, purified, and labeled receptors; S.B., A.F., and W.E.M. analyzed data and wrote the paper.

■ ACKNOWLEDGMENT

■ ADDITIONAL NOTE

■ REFERENCES

(1) Pierce, K. L.; Premont, R. T.; Lefkowitz, R. J. Seven-Transmembrane Receptors. *Nat. Rev. Mol. Cell Biol.* **2002**, *3*, 639–650.

(2) Rosenbaum, D. M.; Rasmussen, S. G. F.; Kobilka, B. K. The Structure and Function of G-Protein-Coupled Receptors. *Nature* **2009**, *459*, 356–363.

(3) Kenakin, T. Efficacy at G-Protein-Coupled Receptors. *Nat. Rev. Drug Discovery* **2002**, *1*, 103–110.

(4) Kenakin, T. P. Cellular Assays as Portals to Seven-Transmembrane Receptor-Based Drug Discovery. *Nat. Rev. Drug Discovery* **2009**, *8*, 617–626.

(5) Frauenfelder, H.; Parak, F.; Young, R. D. Conformational Substates in Proteins. *Annu. Rev. Biophys. Biophys. Chem.* **1988**, *17*, 451–479.

(6) Henzler-Wildman, K.; Kern, D. Dynamic Personalities of Proteins. *Nature* **2007**, *450*, 964–972.

(7) Park, P. S. H.; Lodowski, D. T.; Palczewski, K. Activation of G Protein-Coupled Receptors: Beyond Two-State Models and Tertiary Conformational Changes. *Annu. Rev. Pharmacol. Toxicol.* **2008**, *48*, 107–141.

(8) Vilardaga, J.-P.; Steinmeyer, R.; Harms, G. S.; Lohse, M. J. Molecular Basis of Inverse Agonism in a G Protein-Coupled Receptor. *Nat. Chem. Biol.* **2005**, *1*, 25–28.

(9) Swaminath, G.; Xiang, Y.; Lee, T. W.; Steenhuis, J. J.; Parnot, C.; Kobilka, B. K. Sequential Binding of Agonists to the Beta-2-Adrenoreceptor. *J. Biol. Chem.* **2004**, *279*, 686–691.

(10) Gaertner, H.; Cerini, F.; Escola, J.; Kuenzi, G.; Melotti, A.; Offord, R.; Rossitto-Borlat, I.; Nedellec, R.; Salkowitz, J.; Gorochov, G.; Mosier, D.; Hartley, O. Highly Potent, Fully Recombinant Anti-HIV Chemokines: Reengineering a Low-Cost Microbicide. *Proc. Natl. Acad. Sci. U.S.A.* **2008**, *105*, 17706–17711.

(11) Vilardaga, J.-P.; Bünemann, M.; Krasel, C.; Castro, M.; Lohse, M. J. Measurement of the Millisecond Activation Switch of G Protein-Coupled Receptors in Living Cells. *Nat. Biotechnol.* **2003**, *21*, 807–812.

(12) Bokoch, M. P.; Zou, Y.; Rasmussen, S. G. F.; Liu, C. W.; Nygaard, R.; Rosenbaum, D. M.; Fung, J. J.; Choi, H.-J.; Thian, F. S.; Kobilka, T. S.; et al. Ligand-Specific Regulation of the Extracellular Surface of a G-Protein-Coupled Receptor. *Nature* **2010**, *463*, 108–112.

(13) Sprang, S. R. Cell Signalling: Binding the Receptor at both Ends. *Nature* **2011**, *469*, 172–3.

(14) Rasmussen, S. G. F.; Choi, H.; Rosenbaum, D. M.; Kobilka, T. S.; Thian, F. S.; Edwards, P. C.; Burghammer, M.; Ratnala, V. R. P.; Sanishvili, R.; Fischetti, R. F.; Schertler, G. F. X.; Weis, W. I.; Kobilka, B. K. Crystal Structure of the Human Beta 2 Adrenergic G-Protein-Coupled Receptor. *Nature* **2007**, *450*, 383–387.

(15) Cherezov, V.; Rosenbaum, D. M.; Hanson, M. A.; Rasmussen, S. G. F.; Thian, F. S.; Kobilka, T. S.; Choi, H.-J.; Kuhn, P.; Weis, W. I.; Kobilka, B. K.; Stevens, R. C. High-Resolution Crystal Structure of an Engineered Human Beta 2-Adrenergic G Protein-Coupled Receptor. *Science* **2007**, *318*, 1258–1265.

(16) Rosenbaum, D. M.; Cherezov, V.; Hanson, M. A.; Rasmussen, S. G. F.; Thian, F. S.; Kobilka, T. S.; Choi, H.-J.; Yao, X.-J.; Weis, W. I.; Stevens, R. C.; Kobilka, B. K. GPCR Engineering Yields High-Resolution Structural Insights into Beta 2-Adrenergic Receptor Function. *Science* **2007**, *318*, 1266–1273.

(17) Warne, T.; Serrano-Vega, M. J.; Baker, J. G.; Moukhametzianov, R.; Edwards, P. C.; Henderson, R.; Leslie, A. G. W.; Tate, C. G.;

13336

dx.doi.org/10.1021/jp204843r |*J. Phys. Chem. B* 2011, 115, 13328–13338

Schertler, G. F. X. Structure of a Beta 1-Adrenergic G-Protein-Coupled Receptor. *Nature* 2008, *454*, 486–491.

(18) Jaakola, V.; Griffith, M. T.; Hanson, M. A.; Cherezov, V.; Chien, E. Y. T.; Lane, J. R.; Ijzerman, A. P.; Stevens, R. C. The 2.6 Angstrom Crystal Structure of a Human A2A Adenosine Receptor Bound to an Antagonist. *Science* 2008, *322*, 1211–1217.

(19) Chien, E. Y. T.; Liu, W.; Zhao, Q. A.; Katritch, V.; Han, G. W.; Hanson, M. A.; Shi, L.; Newman, A. H.; Javitch, J. A.; Cherezov, V.; Stevens, R. C. Structure of the Human Dopamine D3 Receptor in Complex with a D2/D3 Selective Antagonist. *Science* 2010, *330*, 1091–1095.

(20) Wu, B. L.; Chien, E. Y. T.; Mol, C. D.; Fenalti, G.; Liu, W.; Katritch, V.; Abagyan, R.; Brooun, A.; Wells, P.; Bi, F. C.; Hamel, D. J.; Kuhn, P.; Handel, T. M.; Cherezov, V.; Stevens, R. C. Structures of the CXCR4 Chemokine GPCR with Small-Molecule and Cyclic Peptide Antagonists. *Science* 2010, *330*, 1066–1071.

(21) Rasmussen, S. G. F.; Choi, H.-J.; Fung, J. J.; Pardon, E.; Casarosa, P.; Chae, P. S.; DeVree, B. T.; Rosenbaum, D. M.; Thian, F. S.; Kobilka, T. S.; et al. Structure of a Nanobody-Stabilized Active State of the Beta 2 Adrenoceptor. *Nature* 2011, *469*, 175–180.

(22) Rosenbaum, D. M.; Zhang, C.; Lyons, J. A.; Holl, R.; Aragao, D.; Arlow, D. H.; Rasmussen, S. G. F.; Choi, H.-J.; DeVree, B. T.; Sunahara, R. K.; et al. Structure and Function of an Irreversible Agonist-Beta 2 Adrenoceptor Complex. *Nature* 2011, *469*, 236–240.

(23) Warne, T.; Moukhametzianov, R.; Baker, J. G.; Nehme, R.; Edwards, P. C.; Leslie, A. G. W.; Schertler, G. F. X.; Tate, C. G. The Structural Basis for Agonist and Partial Agonist Action on a Beta 1-Adrenergic Receptor. *Nature* 2011, *469*, 241–244.

(24) Blanpain, C.; Vanderwinden, J.-P.; Cihak, J.; Wittamer, V.; Le Poul, E.; Issafras, H.; Stangassinger, M.; Vassart, G.; Marullo, S.; Schlöndorff, D.; Parmentier, M.; Mack, M. Mulitple Active States and Oligomerization of CCR5 Revealed by Functional Properties of Monoclonal Antibodies. *Mol. Biol. Cell* 2002, *13*, 723–737.

(25) Ghanouni, P.; Steenhuis, J. J.; Farrens, D. L.; Kobilka, B. K. Agonist-Induced Conformational Changes in the G-Protein-Coupling Domain of the Beta-2-Adrenergic Receptor. *Proc. Natl. Acad. Sci. U.S.A.* 2001, *98*, 5997–6002.

(26) Yao, X. J.; Ruiz, G. V.; Whorton, M. R.; Rasmussen, S. G. F.; DeVree, B. T.; Deupi, X.; Sunahara, R. K.; Kobilka, B. The Effect of Ligand Efficacy on the Formation and Stability of a GPCR-G Protein Complex. *Proc. Natl. Acad. Sci. U.S.A.* 2009, *106* (9501−9506), S9501/1−S9501/3.

(27) Weiss, S. Fluorescence Spectroscopy of Single Biomolecules. *Science* 1999, *283*, 1676–1683.

(28) Moerner, W. E. New Directions in Single-Molecule Imaging and Analysis. *Proc. Natl. Acad. Sci. U.S.A.* 2007, *104*, 12596–12602.

(29) Ying, L. M. Single Molecule Biology: Coming of Age. *Mol. Biosyst.* 2007, *3*, 377–380.

(30) Blank, K.; Rocha, S.; de Cremer, G.; Roeffaers, M. B. J.; Uji-i, H.; Hofkens, J. Watching Individual Enzymes at Work. *Springer Ser. Chem. Phys.* 2010, *96*, 495–511.

(31) Michalet, X.; Weiss, S.; Jager, M. Single-Molecule Fluorescence Studies of Protein Folding and Conformational Dynamics. *Chem. Rev.* 2006, *106*, 1785–1813.

(32) Yang, H.; Luo, G.; Karnchanaphanurach, P.; Louie, T.; Rech, I.; Cova, S.; Xun, L.; Xie, X. S. Protein Conformational Dynamics Probed by Single-Molecule Electron Transfer. *Science* 2003, *302*, 262–266.

(33) Li, C. B.; Yang, H.; Kornatsuzaki, T. Multiscale Complex Network of Protein Conformational Fluctuations in Single-Molecule Time Series. *Proc. Natl. Acad. Sci. U.S.A.* 2008, *105*, 536–541.

(34) Sorokina, M.; Koh, H.; Patel, S. S.; Ha, T. Fluoresecent Lifetime Trajectories of a Single Fluorophore Reveal Reaction Intermediates during Transcription Initiation. *J. Am. Chem. Soc.* 2009, *131*, 9630–9631.

(35) Gansen, A.; Valeri, A.; Hauger, F.; Felekyan, S.; Kalinin, S.; Toth, K.; Langowski, J.; Seidel, C. A. M. Nucleosome Disassembly Intermediates Characterized by Single-Molecule FRET. *Proc. Natl. Acad. Sci. U.S.A.* 2009, *106*, 15308–15313.

(36) Santoso, Y.; Joyce, C. M.; Potapova, O.; Le Reste, L.; Hohlbein, J.; Torella, J. P.; Grindley, N. D. F.; Kapanidis, A. N. Conformational Transitions in DNA Polymerase I Revealed by Single-Molecule FRET. *Proc. Natl. Acad. Sci. U.S.A.* 2010, *107*, 715–720.

(37) Rasnik, I.; McKinney, S. A.; Ha, T. Surfaces and Orientations: Much to FRET about? *Acc. Chem. Res.* 2005, *38*, 542–548.

(38) Ashkin, A.; Dziedzic, J. M.; Bjorkholm, J. E.; Chu, S. Observation of a Single-Beam Gradient Force Optical Trap for Dielectric Particles. *Opt. Lett.* 1986, *11*, 288–290.

(39) Cohen, A. E.; Moerner, W. E. Suppressing Brownian Motion of Individual Biomolecules in Solution. *Proc. Natl. Acad. Sci. U.S.A.* 2006, *103*, 4362–4365.

(40) Cohen, A. E.; Moerner, W. E. Principal-Components Analysis of Shape Fluctuations of Single DNA Molecules. *Proc. Natl. Acad. Sci. U.S.A.* 2007, *104*, 12622–12627.

(41) Cohen, A. E.; Moerner, W. E. Controlling Brownian Motion of Single Protein Molecules and Single Fluorophores in Aqueous Buffer. *Opt. Express* 2008, *16*, 6941–6956.

(42) Goldsmith, R. H.; Moerner, W. E. Watching Conformational- and Photodynamics of Single Fluorescent Proteins in Solution. *Nat. Chem.* 2010, *2*, 179–186.

(43) Fields, A. P.; Cohen, A. E. Anti-Brownian Traps for Studies on Single Molecules. *Methods Enzymol.* 2010, *475*, 149–174.

(44) Wang, Q.; Moerner, W. E. An Adaptive Anti-Brownian ELectrokinetic (ABEL) Trap with Real-Time Information on Single-Molecule Diffusivity and Mobility. *ACS Nano* 2011, *5*, 5792–5799.

(45) Fields, A. P.; Cohen, A. E. Electrokinetic Trapping at the One Nanometer Limit. *Proc. Nat. Acad. Sci. U.S.A.* 2011, DOI: 10.1073/pnas.1103554108.

(46) Rigler, R.; Elson, E., Eds. In *Fluorescence Correlation Spectroscopy*; Schaefer, F. P., Toennies, J. P., Zinth, W., Eds.; Springer Series in Chemical Physics; Springer: Berlin, 2001; Vol. 65, p 487.

(47) Eggeling, C.; Fries, J. R.; Brand, L.; Gunther, R.; Seidel, C. A. M. Monitoring Conformational Dynamics of a Single Molecule by Selective Fluorescence Spectroscopy. *Proc. Natl. Acad. Sci. U.S.A.* 1998, *95*, 1556–1561.

(48) Vogel, M.; Rettig, W.; Sens, R.; Drexhage, K. H. Structural Relaxation of Rhodamine Dyes with Different N-Substitution Patterns - a Study of Fluorescence Decay Times and Quantum Yields. *Chem. Phys. Lett.* 1988, *147*, 452–460.

(49) Devanathan, S.; Yao, Z.; Salamon, Z.; Kobilka, B. K.; Tollin, G. Plasmon-Waveguide Resonance Studies of Ligan Binding to the Human Beta-2-Adrenergic Receptor. *Biochemistry* 2004, *43*, 3280–3288.

(50) Peleg, G.; Ghanouni, P.; Kobilka, B. K.; Zare, R. N. Single-Molecule Spectroscopy of the Beta-2 Adrenergic Receptor: Observation of Conformational Substates in a Membrane Protein. *Proc. Natl. Acad. Sci. U.S.A.* 2001, *98*, 8469–8474.

(51) Yao, X. J.; Parnot, C.; Deupi, X.; Ratnala, V. R. P.; Swaminath, G.; Farrens, D.; Kobilka, B. Coupling Ligand Structure to Specific Conformational Switches in the Beta(2)-Adrenoceptor. *Nat. Chem. Biol.* 2006, *2*, 417–422.

(52) Fischer, M.; Georges, J. Fluorescence Quantum Yield of Rhodamine 6G in Ethanol as a Function of Concentration using Thermal Lens Spectrometry. *Chem. Phys. Lett.* 1996, *260*, 115–118.

(53) Lakowicz, J. R. In *Principles of Fluorescence Spectroscopy*; Kluwer Academic: New York, 1999.

(54) Cohen, A. E.; Moerner, W. E. The Anti-Brownian Electrophoretic Trap (ABEL Trap): Fabrication and Software. *Proc. SPIE—Int. Soc. Opt. Eng.* 2005, *5699*, 296–305.

(55) Jiang, Y.; Wang, Q.; Cohen, A. E.; Douglas, N.; Frydman, J.; Moerner, W. E. Hardware-Based Anti-Brownian Electrokinetic Trap (ABEL Trap) for Single Molecules: Control Loop Simulations and Application to ATP Binding Stoichiometry in Multi-Subunit Enzymes. *Proc. Soc. Photo Opt. Instrum. Eng.* 2008, *7038*, 703807.

(56) Watkins, L. P.; Yang, H. Detection of Intensity Change Points in Time-Resolved Single-Molecule Measurements. *J. Phys. Chem. B* 2005, *109*, 617–628.

(57) Zander, C.; Sauer, M.; Drexhage, K. H.; Ko, D.-S.; Schulz, A.; Wolfrum, J.; Brand, L.; Eggeling, C.; Seidel, C. A. M. Detection and

13337

dx.doi.org/10.1021/jp204843r |*J. Phys. Chem. B* 2011, 115, 13328–13338

Characterization of Single Molecules in Aqueous Solution. *Appl. Phys. B* **1996**, *63*, 517–523.

(58) Baptista, M. S.; Indig, G. L. Effect of BSA Binding on Photophysical and Photochemical Properties of Triarylmethane Dyes. *J. Phys. Chem. B* **1998**, *102*, 4678–4688.

(59) Fürstenberg, A.; Kel, O.; Gradinaru, J.; Ward, T. R.; Emery, D.; Bollot, G.; Mareda, J.; Vauthey, E. Site-Dependent Excited-State Dynamics of a Fluorescent Probe Bound to Avidin and Streptavidin. *ChemPhysChem* **2009**, *10*, 1517–1532.

(60) Wlodarczyk, J.; Kierdaszuk, B. Interpretation of Fluorescence Decays using a Power-Like Model. *Biophys. J.* **2003**, *85*, 589–598.

(61) Siemiarczuk, A.; Wagner, B. D.; Ware, W. R. Comparison of the Maximum Entropy and Exponential Series Methods for the Recovery of Distributions of Lifetimes from Fluorescence Lifetime Data. *J. Phys. Chem.* **1990**, *94*, 1661–6.

(62) Kinosita, K., Jr.; Kawato, S.; Ikegami, A. A Theory of Fluorescence Polarization Decay in Membranes. *Biophys. J.* **1977**, *20*, 289–305.

(63) Lipari, G.; Szabo, A. Effect of Librational Motion on Fluorescence Depolarization and Nuclear Magnetic Resonance Relaxation in Macromolecules and Membranes. *Biophys. J.* **1980**, *30*, 489–506.

(64) Schwille, P.; Kummer, S.; Heikal, A. A.; Moerner, W. E.; Webb, W. W. Fluorescence Correlation Spectroscopy Reveals Fast Optical Excitation-Driven Intermolecular Dynamics of Yellow Fluorescent Proteins. *Proc. Natl. Acad. Sci. U.S.A.* **2000**, *97*, 151–156.

(65) Box, G. E. P.; Jenkins, G. M. In *Time Series Analysis forecasting and control*; Holden-Day, Inc.: San Francisco, CA, 1970.

(66) Dickson, R. M.; Cubitt, A. B.; Tsien, R. Y.; Moerner, W. E. On/Off Blinking and Switching Behavior of Single Green Fluorescent Protein Molecules. *Nature* **1997**, *388*, 355–358.

(67) Hanson, J.; Yang, H. A General Statistical Test for Correlations in a Finite-Length Time Series. *J. Chem. Phys.* **2008**, *128*, 214101.

(68) Chung, S. H.; Stevens, J. R. Time-Dependent Correlation and the Evaluation of the Stretched Exponential Or Kohlrausch-Williams-Watts Function. *Am. J. Phys.* **1991**, *59*, 1024–1030.

(69) Lu, C.-Y.; VandenBout, D. A. Effect of Finite Trajectory Length on the Correlation Function Analysis of Single Molecule Data. *J. Chem. Phys.* **2006**, *125*, 124701-1–124701-9.

(70) Neumann, L.; Wohland, T.; Whelan, R. J.; Zare, R. N.; Kobilka, B. K. Functional Immobilization of a Ligand-Activated G-Protein-Coupled Receptor. *ChemBioChem* **2002**, *3*, 993–998.

(71) Swaminath, G.; Deupi, X.; Lee, T. W.; Zhu, W.; Thian, F. S.; Kobilka, T. S.; Kobilka, B. Probing the Beta(2) Adrenoceptor Binding Site with Catechol Reveals Differences in Binding and Activation by Agonists and Partial Agonists. *J. Biol. Chem.* **2005**, *280*, 22165–22171.

(72) Nau, W. M.; Hennig, A.; Koner, A. L. Squeezing Fluorescent Dyes into Nanoscale Containers-the Supramolecular Approach to Radiative Decay Engineering. *Springer Ser. Fluoresc.* **2008**, *4*, 185–211.

(73) Stracke, F.; Blum, C.; Becker, S.; Mullen, K.; Meixner, A. J. Correlation of Emission Intensity and Spectral Diffusion in Room Temperature Single-Molecule Spectroscopy. *ChemPhysChem* **2005**, *6*, 1242–1246.

(74) Watanabe, K.; Klein, M. L. Shape Fluctuations in Ionic Micelles. *J. Phys. Chem.* **1989**, *93*, 6897–6901.

(75) Halle, B.; Landgren, M.; Jonsson, B. The Shape of Ionic Micelles. *J. Phys. (Paris)* **1988**, *49*, 1235–1259.

(76) Bond, P. J.; Cuthbertson, J. M.; Deol, S. S.; Sansom, M. S. P. MD Simulations of Spontaneous Membrane protein/detergent Micelle Formation. *J. Am. Chem. Soc.* **2004**, *126*, 15948–15949.

(77) Dror, R. O.; Arlow, D. H.; Borhani, D. W.; Jensen, M. O.; Piana, S.; Shaw, D. E. Identification of Two Distinct Inactive Conformations of the Beta(2)-Adrenergic Receptor Reconciles Structural and Biochemical Observations. *Proc. Natl. Acad. Sci. U.S.A.* **2009**, *106*, 4689–4694.

13338

dx.doi.org/10.1021/jp204843r |*J. Phys. Chem. B* 2011, 115, 13328–13338